Available online at www.sciencedirect.com
ScienceDirect
Nuclear Instruments and Methods in Physics Research A 587 (2008) 13–19
NUCLEAR INSTRUMENTS & METHODS IN PHYSICS RESEARCH Section A
www.elsevier.com/locate/nima

Measurement of NdFeB permanent magnets demagnetization induced by high energy electron radiation ☆

Alexander B. Temnykh*

Wilson Lab, Cornell University, LEPP, Ithaca, NY 14850, USA

Received 26 December 2007; received in revised form 2 January 2008; accepted 3 January 2008
Available online 6 January 2008

Abstract

Demagnetization of NdFeB permanent magnets has been measured as function of radiation dose induced by high energy electrons. The magnet samples were of different intrinsic coercive forces, $\simeq 12$ and $\simeq 20$ KOe, dimensions and direction of magnetization. 5 GeV electron beam from 12 GeV Cornell Synchrotron was used as a radiation source. A calorimetric technique was employed for radiation dose measurement. Results indicated that depending on the sample intrinsic coercive force, shape and direction of magnetization the radiation dose causing 1% of demagnetization of the sample varies from 0.0765 ± 0.005 Mrad to 11.3 ± 3.0 Mrad, i.e., by more than a factor of 100.

Experimental data analysis revealed that demagnetization of the given sample induced by radiation is strongly correlated with the sample demagnetizing temperature. This correlation was approximated by an exponential function with two parameters obtained from the data fitting. The function can be used to predict the critical radiation dose for permanent magnet assemblies like undulator magnets based on its demagnetizing temperature. The latter (demagnetization temperature) can be determined at the design stage from 3-D magnetic modeling and permanent magnet material properties.
Published by Elsevier B.V.

PACS: 75.50.Ww

Keywords: Demagnetization; Magnetic field; NdFeB magnet; Undulator; Electron beam; Radiation

1. Introduction

Demagnetization of permanent magnet (PM) material induced by radiation is a great concern in the design of insertion devices (ID). The strength of the ID magnetic field, X-ray intensity and spectrum depend on the ID gap. A smaller ID gap results in stronger magnetic field, higher X-ray intensity and wider operation range. All these choices make ID operation more efficient. However, the smaller gap increases the risk of ID radiation damage. The number of high energy electrons scattered from the electron beam and absorbed in PM material results in radiation dose and increases rapidly when the gap decreases. With time, PM demagnetization induced by radiation degrades the ID performance, see Ref. [1]. The accurate knowledge of the dependence of PM demagnetization on radiation doses could help one optimize ID design for the required ID life time and given operation conditions.

Refs. [2–4] describe the measurement of the dependence of radiation-induced demagnetization on radiation dose for several PM materials. The data indicate that the demagnetization depends not only on radiation dose, but also on PM material intrinsic coercive force, sample dimensions, magnetic environment, heat treatment prior to irradiation, sample temperature at the moment of irradiation and many other factors. The complicity of the problem is well illustrated in Ref. [5].

The variety of factors affecting demagnetization as well as a wide spread of radiation characteristics among studied PM materials suggest that the published to date data can

☆ Work supported by the National Science Foundation under Contract PHY 0202078.

*Tel.: +1 607 255 4882; fax: +1 607 255 8062.
E-mail address: abt6@cornell.edu

0168-9002/$ - see front matter Published by Elsevier B.V.
doi:10.1016/j.nima.2008.01.002

be used only as a strategic guidance. To evaluate specific PM material one should test it in conditions close to what are expected in operation. This was a motivation for the experiments described below. The PM material as well as dimensions of the tested samples were similar to those of which we are planning to use in construction of insertion device for Cornell Energy Recovery Linac (ERL) synchrotron radiation source. As a radiation source we used 5 GeV electrons beam from 12 GeV Cornell Synchrotron which simulated high energy electrons scattered from the ERL beam.

Table 1
Characteristics of the tested NdFeB PM materials

Grade	Br (KGs)	Hc (KOe)	Hci (KOe)	(BH)max (MGOe)
$N40$	12.5–12.8	$\geqslant$11.6	$\geqslant$12	38–41
$N40SH$	12.4–12.8	$\geqslant$11.8	$\geqslant$20	38–41

2. PM material and the tested samples properties

$N40$ and $N40SH$ grades of NdFeB PM material delivered by "Stanford Magnets Company" were used in the radiation test. These grades have different intrinsic coercive forces, see Table 1, resulting in quite different dependence of demagnetization on temperature, see demagnetization curves depicted in Fig. 1.

The tested samples were rectangular blocks with dimensions summarized in Table 2. Samples had two types of magnetization direction. "V" samples were magnetized in 0.5 in., "vertical", and "H" samples were magnetized in 0.125 in. ($N40$) and in 0.25 in. ($N40SH$), "horizontal" directions. To increase reliability of the measurement, two identical samples of each type were tested.

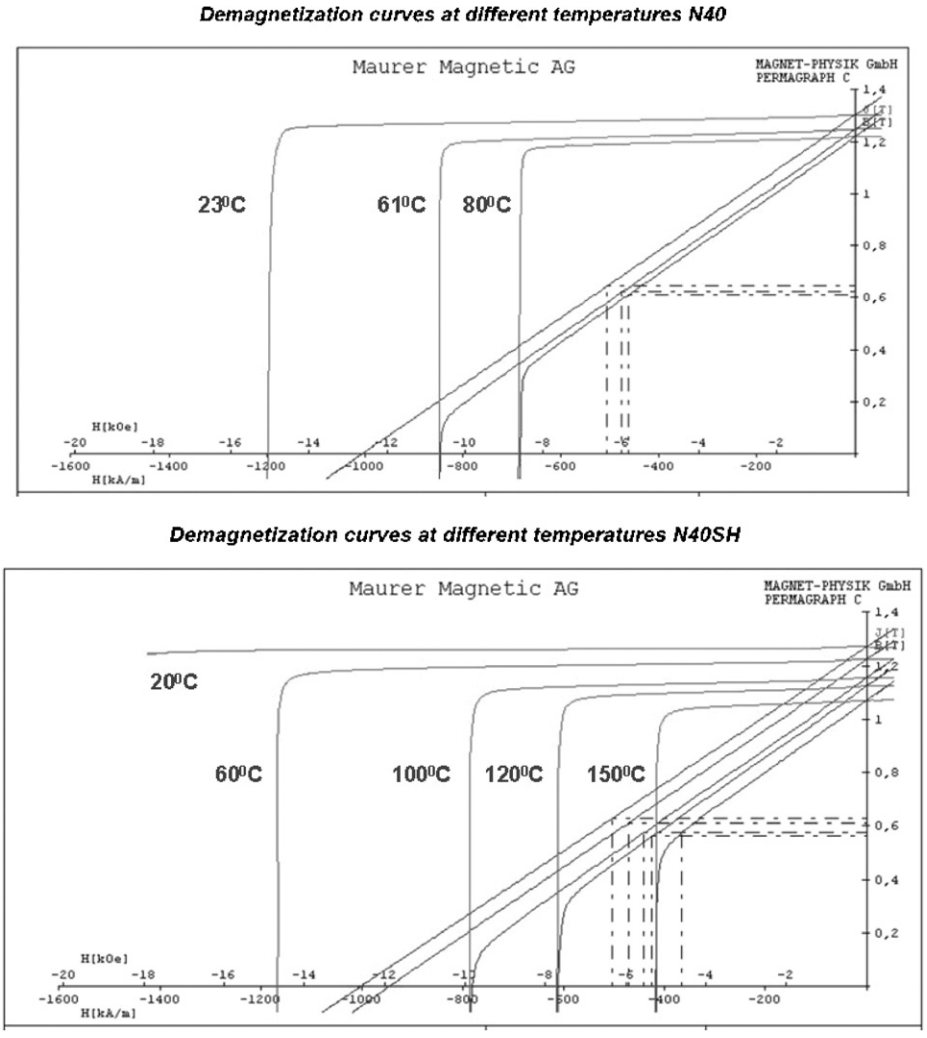

Fig. 1. $N40$ and $N40SH$ demagnetization curves at different temperature, copied from website: www.maurermagnetic.ch. The curves show intrinsic magnetization and intrinsic magnetic field as functions of magnetic field induction. Knees in curves indicate points where PM material becomes permanently demagnetized.

For each type of sample we evaluated demagnetizing temperature, i.e., temperature at which the given sample would be permanently demagnetized. The procedure is outlined below:

First, using 3D magnetic modeling software [6], the minimum intrinsic magnetic field in the direction of magnetization was found, then demagnetizing temperature was determined from curves depicted in Fig. 1. Minimum intrinsic field and demagnetizing temperature for each type of samples are given in Table 3.

Comparing samples of the same PM material grade and dimensions but with different direction of magnetization, one can notice a significant difference in the minimum intrinsic field and as a result of it in demagnetization temperature. For example, $N40$ grade "H" block has minimum field 1.55 kG and demagnetization temperature 61.6 °C while "V" block has 6.3 kG of minimum field and much higher demagnetization temperature ~114.6 °C. This difference is solely due to a geometrical factor translating into a different intrinsic demagnetizing magnetic induction, see Fig. 2.

Higher demagnetization temperatures for samples of $N40SH$ grade when compare with $N40$ are mostly due to higher coercive forces.

Table 2
The tested samples properties

Sample	Dimension $W \times H \times L$ (in.)	Dir of mag.	Qty.
$N40, V$	$1.0 \times 0.5 \times 0.125$	0.500	2
$N40, H$	$1.0 \times 0.5 \times 0.125$	0.125	2
$N40SH, V$	$1.0 \times 0.5 \times 0.25$	0.500	2
$N40SH, H$	$1.0 \times 0.5 \times 0.25$	0.250	2

Table 3
Calculated minimum intrinsic field and demagnetization temperature for the tested PM samples

PM grade, block type	Min. int. field (kG)	Demag. temp. (°C)
$N40, H$	1.55	61.66
$N40, V$	6.33	114.6
$N40SH, H$	3.88	128.8
$N40SH, V$	5.83	149.5

3. Experimental setup and measurement procedure

For irradiation, four PM blocks were stacked in the assembly depicted in Fig. 3. To reduce the reciprocal influence of the magnetic field of the adjacent blocks, they were separated by 1 in. copper spacers. The assembly was attached to a straight section of the East transfer beam line connecting the 12 GeV Synchrotron with Cornell Electron Storage Ring as is schematically shown in Fig. 4. A 5 GeV electron beam coming from 12 GeV Synchrotron was

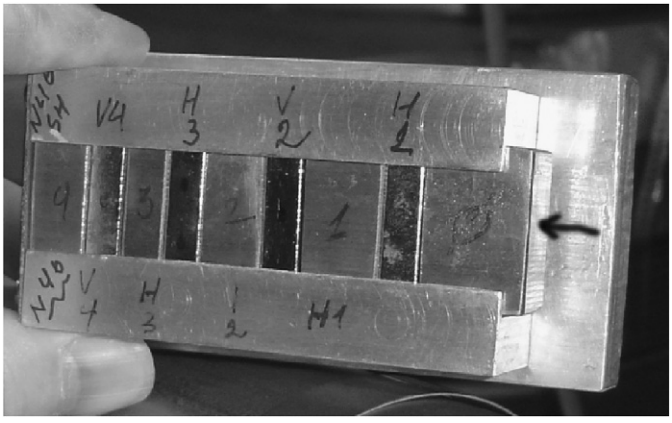

Fig. 3. PM block assembly. Arrow shows the high energy electron beam direction.

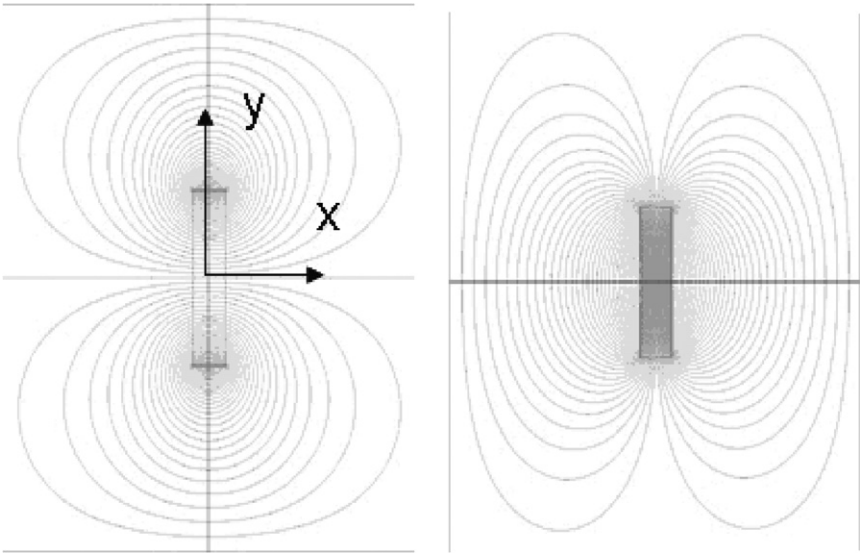

Fig. 2. "H" (left) and "V" (right) type of block magnetic field geometry. The line density proportional to the magnetic field strength. X- and Y- axes indicate horizontal and vertical directions.

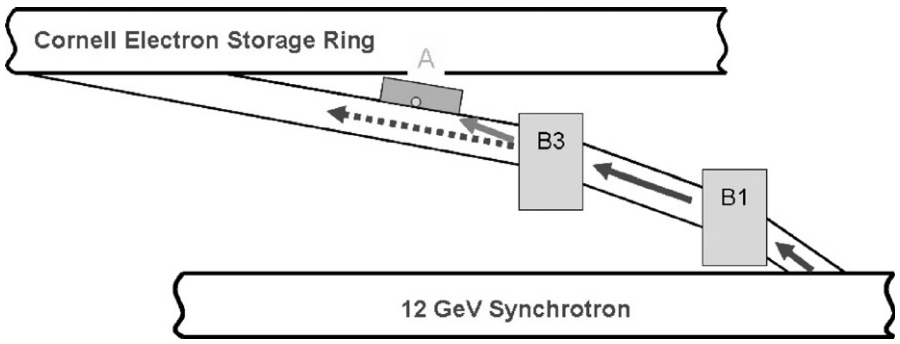

Fig. 4. East transfer line schema. $B1$ and $B3$ are bending magnets. A—the assemble location.

steered with a bending magnet "B3" to the PM assembly location. At this location the beam pipe was a round stainless steel tube with 100 mm diameter and ~1 mm thickness. The immediate response to the radiation was a temperature rise of the assembly and a signal from radiation monitors positioned nearby assembly. The temperature change was used for radiation dose measurement.

The measurement sequence consisted of the magnetic measurements and irradiation. First, the magnetic moment of each PM block was accurately measured with a Helmholtz coil apparatus. Then, the blocks were assembled in a structure shown in Fig. 3. The assembly was moved to the CESR tunnel and attached to the East transfer line. After irradiation, we waited a couple of days to allow residual radiation of the assembly to decay to a safe level. The assembly was then retrieved from the tunnel, taken apart, and the magnetic moment of each PM block was measured again. Radiation dose was calculated from the assembly temperature variation during irradiation as described below. This cycle was repeated till a few percent of the PM sample magnetic moment loss was detected.

4. Radiation dose measurement technique

One example of the assembly temperature variation during the irradiation cycle is depicted in Fig. 5. The temperature was monitored by two attached thermocouple sensors. The plot shows a ~5 °C temperature rise when electron beam was directed to the assembly location, (period 1), and cooling down process, (period 2), with electron beam turned off. The rise of the assembly temperature is caused by the absorbed energy of electron beam, i.e., by the radiation dose.

Noting that the radiation dose, by definition, is the amount of energy absorbed per unit of mass, one can easily find the dose from the assembly temperature change in the following way.

The dependence of the assembly temperature on time, $T(t)$, can be described by the equation:

$$\frac{dT}{dt} = \frac{Q}{C} - \frac{T - T_0}{\tau} \quad (1)$$

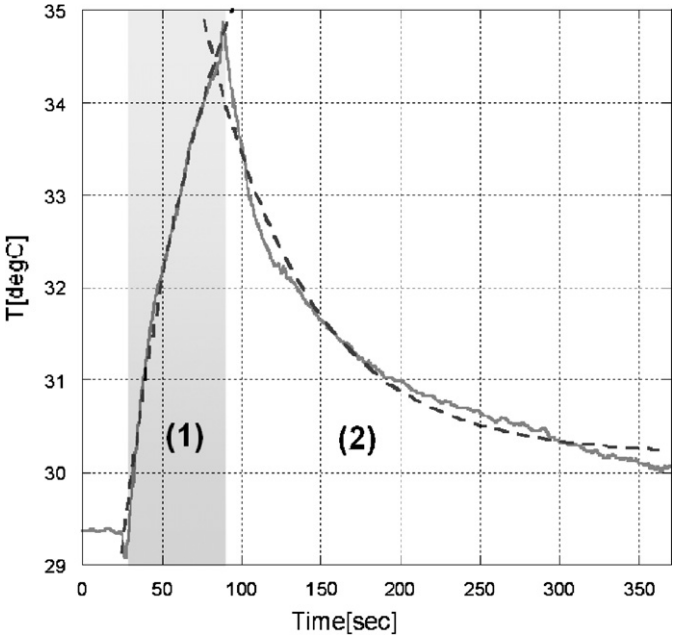

Fig. 5. PM assembly temperature variation during irradiation cycle. Shaded area indicates period with electron beam turned on. Cooling occurs during period 2, with electron beam turned off. Dashed line shows fitting according to expressions (2) and (3), see text.

where Q is the energy absorption rate per unit mass, i.e., radiation dose rate, C the material specific heat capacity, τ the cooling time constant, T_0 the ambient temperature. Specific heat capacities for the NdFeB PM blocks and cooper spacers are 0.44 and 0.39 J/g/°C, respectively. Because they differ by only 10%, one can use an average number of 0.41 J/g/°C without introducing a large error. The solution of Eq. (1) for the temperature rise during irradiation, (period 1) is

$$T = T_0 + \tau \frac{Q}{C}(1 - \exp(-t/\tau)) \quad (2)$$

and cooling down (period 2):

$$T = T_0 + \Delta T \cdot \exp(-t/\tau). \quad (3)$$

A fit of the observed temperature variation according to expressions (2) and (3), (see dashed line in Fig. 5), gives the

cooling time constant:

$$\tau = 64.5 \pm 0.97\,\mathrm{s} \tag{4}$$

and

$$Q/C = 0.131 \pm 0.001\,^{\circ}\mathrm{C/s}. \tag{5}$$

For given specific heat capacities $0.41\,\mathrm{J/g/^{\circ}C}$, the energy absorption rate, i.e., radiation dose rate, will be:

$$Q = 0.054\,\mathrm{J/g/s} = 5.4 \times 10^3\,\mathrm{rad/s}. \tag{6}$$

Sixty seconds of irradiation time, see period 1 in Fig. 5, yield an accumulated radiation dose:

$$D = 5.4 \times 10^3\,\mathrm{rad/s} \times 60\,\mathrm{s} = 0.324\,\mathrm{Mrad}. \tag{7}$$

To avoid magnetic material demagnetization caused by high temperature, the temperature rise during irradiation was purposely kept below ~5 °C by controlling the electron beam intensity and the irradiation time. Thus, to accumulate the desired dose, it was necessary to make a number of cycles. For example, Fig. 6 shows the assembly temperature variation during irradiation on November 15 2006. Here one can see 11 cycles which resulted in 3.2 Mrad of total radiation dose accumulation.

Since the electron beam has a limited transfer dimension, the radiation dose distribution over the sample can be non-uniform. One can raise the question what is the effect of this non-uniformity on the measurement result? In fact, the use of the calorimetric method for the radiation dose measurement and the measurement of the total magnetic moment of the samples minimize this effect. It may be shown in the following way:

The radiation dose, D, measured calorimetrically can be expressed through the radiation dose distribution, $\Psi(x,y,z)$, as

$$D = \frac{1}{V_s}\int \Psi(x,y,z)\,\mathrm{d}V \tag{8}$$

where V_s is the tested sample volume. Since the PM material magnetization loss is linear with radiation dose, (see [2,3] and experimental data below), the equation for relative change of the sample magnetic moment can be written as

$$\frac{\mathrm{d}M}{M} = \frac{\int \mu\alpha\Psi(x,y,z)\,\mathrm{d}V}{\int \mu\,\mathrm{d}V} = \frac{1}{V_s}\int \alpha\Psi(x,y,z)\,\mathrm{d}V \tag{9}$$

where μ is the PM material magnetization and α describes the relative magnetization loss caused by the radiation $\Psi(x,y,z)$. Combining Eqs. (8) and (9) and assuming that α does not vary much over the sample volume, one can find:

$$\frac{(\mathrm{d}M/M)}{D} \sim \alpha. \tag{10}$$

This expression indicates that the ratio between the magnetic moment change and the accumulated dose, $(\mathrm{d}M/M)/D$, does not depend on the distribution of the accumulated radiation dose. In addition, this ratio can be considered as the relative magnetization loss of the PM material caused by radiation at microscopic level.

5. Result

Experimental results are presented in Fig. 7 and in Table 4. Fig. 7 shows dependence of the PM block magnetic moment change as function of accumulated radiation dose. It summarizes the results for all eight

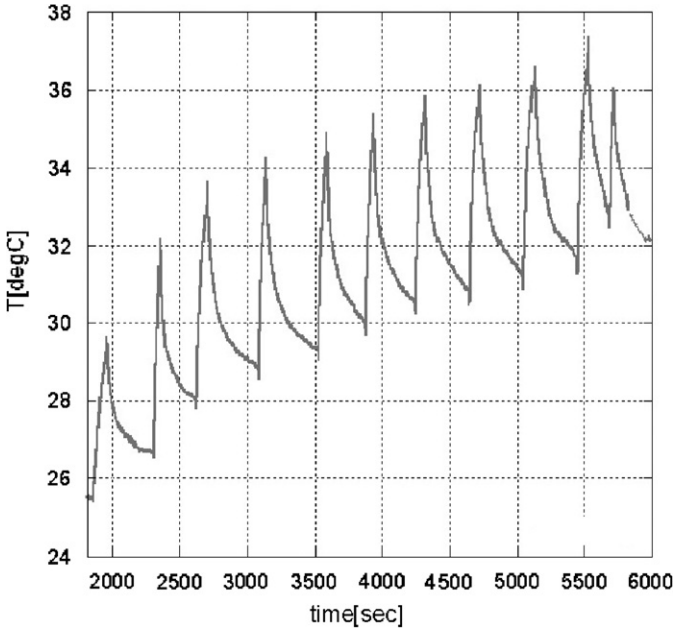

Fig. 6. Assembly temperature variation during irradiation on November 15 2006. One can see 11 cycles resulting the total accumulated dose 3.2 Mrad.

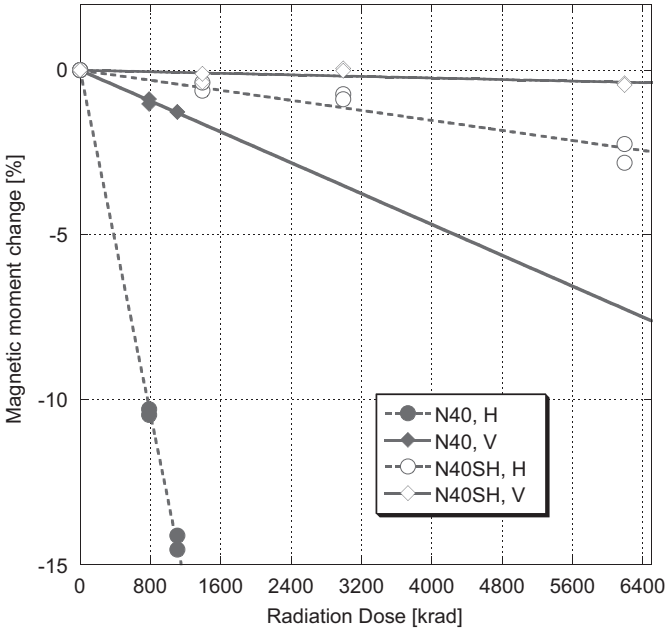

Fig. 7. The measured magnetic moment change as a function of accumulated radiation dose. Solid circles and diamonds are for "H" and "V" blocks of $N40$ grade, open circles and diamonds indicate $N40SH$ "H" and "V" blocks, respectively.

Table 4
The measured radiation dose causing 1% of demagnetization and demagnetization temperature for the tested PM samples

PM grade, block type	1% demagnetization dose (Mrad)	Demag. temp. (°C)
*N*40, *H*	0.0765 ± 0.005	61.66
*N*40, *V*	0.851 ± 0.020	114.6
*N*40*SH*, *H*	2.54 ± 0.17	128.8
*N*40*SH*, *V*	11.3 ± 3.0	149.5

tested PM samples. Here one can see a good consistency between the data for identical samples. Table 4 shows the radiation doses causing 1% of demagnetization for each type of the tested PM blocks obtained from the linear fit of the data depicted in Fig. 7.

Experimental data indicate that "*H*" blocks of the *N*40 grade are most vulnerable to radiation induced demagnetization. For them only 76 ± 5 krad was required to cause 1% magnetization loss. "*V*" blocks are more resistant. The 1% demagnetization dose for them is 851 ± 20 krad, i.e., ~11 times higher. Blocks made of *N*40*SH* grade are more stable against radiation damage. For 1% demagnetization of "*H*" block 2.5 ± 0.17 Mrad is required, and 11.3 ± 3 Mrad for "*V*" block.

Uncertainties of the results given in Table 4 were estimated from the residuals of the linear fitting. The main contributor to the uncertainties was the non-constant temperature at the time of PM block magnetic moment measurement. Temperature variation of ±2 °C at the location of the magnetic measurement lab gives an uncertainty of ±0.24% in the blocks magnetic moment. The relatively large error for "*V*" *N*40*SH* samples is due to small measured magnetization loss even at maximum accumulated radiation dose.

6. Data analysis and discussion

Two important observations can be made from the radiation induced demagnetization data presented in Table 4.

Comparing "*V*" blocks of *N*40*SH* and *N*40 PM grade, one can see that *N*40*SH* grade blocks are 20(!) times more resistant to radiation than *N*40. Because these blocks have very similar geometry and field strength, and defer only by intrinsic coercive forces, one can suggest that the latter (intrinsic coercive force) caused the difference in resistance to radiation demagnetization. This well agrees with the commonly accepted hypothesis that stronger intrinsic coercive forces make PM more resistive to radiation.

Second, comparing "*H*" and "*V*" blocks of the same material grade, one can see that "*V*" blocks can sustain more radiation than ones of "*H*" type. This difference is a factor of 10 for *N*40 and a factor of 6 for *N*40*SH* grade blocks. One explanation of this difference would be the dependence of demagnetization on angle between the PM magnetization direction and the direction of the electron beam as was suggested in Ref. [2] (in our case, "*H*" type block magnetization was parallel to the beam direction while magnetization of "*V*" blocks perpendicular). A different explanation, which is in our opinion more reasonable, is the dependence of the radiation demagnetization on intrinsic demagnetizing magnetic induction, similar to the dependence affecting temperature demagnetization, see discussion in Section 2.

This hypothesis is also supported by the data depicted on Fig. 2(b) in Ref. [2], which compared the effect of radiation demagnetization for the cube and plate shape PM samples. The data indicate that for the samples with parallel direction of magnetization, 30e13 of accumulated electron dose causes ~3.2% of demagnetization of the cube shape sample and ~10.5% (7% more!) demagnetization of the plate sample. Because of the interference between the direction of magnetization and shape, these samples have very different intrinsic demagnetizing magnetic induction. Comparing samples with perpendicular magnetization, which have smaller difference in intrinsic demagnetizing magnetic induction, one can see much smaller difference in demagnetization, ~1%. Note that intrinsic demagnetizing magnetic induction is reflected to some degree by a permeance coefficients $B/\mu_0 H$ depicted for each tested sample on the right side of the figure.

To make a comparison easier between two phenomenon, radiation and temperature induced demagnetization, a column with the demagnetization temperatures, see Table 3, was added to Table 4. One can notice that at qualitative level, the dependence of both phenomenon on the material grade and sample geometry is very similar.

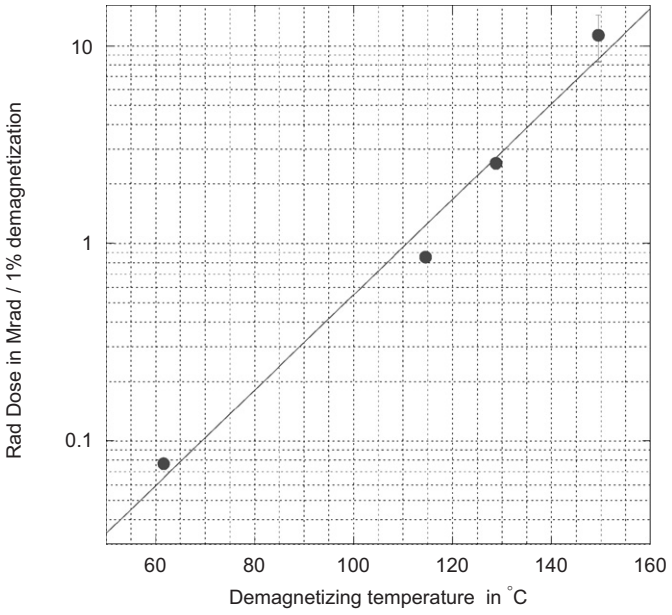

Fig. 8. Radiation dose, D, causing 1% of magnetization loss as function of demagnetization temperature, T_{dmg}. A least-square fit of data to function $\mathrm{Log}_{10}(D(\mathrm{Mrad})) = m_0 + T_{\mathrm{dmg}}(^{\circ}\mathrm{C})/\overline{T}$ gives $m0 = -2.68 \pm 0.28$, $\overline{T} = 41.4 \pm 4\,^{\circ}\mathrm{C}$ with parameter $R = 0.991$.

This similarity can be analyzed phenomenologically. In Fig. 8, radiation doses corresponding to 1% demagnetization, $D_{1\%}$, are plotted against demagnetizing temperatures, T_{dmg}. Each point represents the type of the tested sample. Note that the samples had different intrinsic coercive forces, geometry and direction of magnetization. The vertical axis is in logarithmic scale. The plot reveals a strong linear-like correlation between $\mathrm{Log}(D_{1\%})$ and T_{dmg}. A least-square fit to the function:

$$\mathrm{Log}_{10}(D_{1\%}(\mathrm{Mrad})) = m0 + T_{\mathrm{dmg}}(^{\circ}\mathrm{C})/\overline{T} \tag{11}$$

gives $m0 = -2.68 \pm 0.28$, $\overline{T} = 41.4 \pm 4.0\,^{\circ}\mathrm{C}$ with parameter $R = 0.991$. Rewriting Eq. (11) in form:

$$D_{1\%} = 10^{m0} \times 10^{T_{\mathrm{dmg}}/\overline{T}} \tag{12}$$

one can derive an expression for the sample demagnetization, $\mathrm{d}M/M$, as a function of accumulated radiation dose, D, and demagnetization temperature, T_{dmg}:

$$\frac{\mathrm{d}M}{M} = -0.01\frac{D}{D_{1\%}} = -\frac{D}{D^*} \times 10^{-T_{\mathrm{dmg}}/\overline{T}} \tag{13}$$

where $D^* = 0.25 \pm 0.14\,\mathrm{Mrad}$ and $\overline{T} = 41.4 \pm 4.0\,^{\circ}\mathrm{C}$.

Eq. (13) gives an estimate of demagnetization induced by radiation dose, D, based on demagnetizing temperature, T_{dmg}. T_{dmg}, in turn, can be easily determined from a 3D magnetic model and demagnetization curves for different temperatures for a given PM material, as was done above. Estimation can be done not only for single PM with simple geometry, but also for PM assemblies like undulator magnets. The knowledge of the critical radiation dose for a given undulator design is of great practical importance. It is known that aggressive ID design with a stronger magnetic field in the ID gap usually results in stronger intrinsic demagnetizing induction and lower demagnetizing temperature. This design choice will reduce resistivity to radiation demagnetization, i.e., reduce ID life time. Eq. (13) provides a base for calculable compromise between the aggressiveness of the ID design and the requirement on the ID life time.

It is interesting to compare radiation doses causing demagnetization measured in the presented experiments with data reported elsewhere. In the similar experiments described in Refs. [2,3], it was found that PM samples can lose a few percent of magnetization after being exposed to $\sim 5 \times 10^{14}$ electrons with 2 GeV energy. Assuming electron energy loss rate in PM material $\sim 2\,\mathrm{MeV\,cm^2/g}$ and $7.8\,\mathrm{g/cm^3}$ PM material density, for given $46\,\mathrm{mm} \times 8\,\mathrm{mm} \times 12\,\mathrm{mm}$ samples used for test and electrons traveled in 8 mm directions, one can find the total energy deposited into a sample $\sim 6.25 \times 10^{21}\,\mathrm{eV}$. This corresponds to $\sim 3\,\mathrm{Mrad}$ of a radiation dose. The latter is consistent with doses measured in the presented experiments, see Table 4.

7. Conclusion

NdFeB PM samples with two very different coercive forces, sizes and directions of magnetization were irradiated by high energy electrons and their demagnetization was measured as a function of accumulated radiation dose. A 5 GeV electron beam was used for irradiation and the radiation dose was measured with a calorimetric technique. The measurements were done during CESR operation for CHESS in parasitic mode in October–November of 2006 without disturbing storage ring running.

The data obtained in the experiments revealed a strong correlation between the sample demagnetization induced by radiation and the sample demagnetizing temperature. The correlation was described by exponent function with two parameters obtained from the data fitting. Since the demagnetizing temperature can be determined from magnetic field modeling and PM material characteristics at the ID design stage, using this correlation function one can *predict* the ID's radiation resistance and consequently the ID life time for given operation conditions. This estimate is of great practical importance because it can be used for ID design evaluation as well as for evaluation of requirements on the residual gas density, primary source of radiation at ID location, and on scheme for ID radiation shielding.

The results of the experiments described above are consistent with previously published data.

Acknowledgements

Author would like to thank David Rice and Sol Gruner for support of the described above activity, and express gratitude to Gregori Temnykh for proof reading and editing this paper.

References

[1] S. Sasaki, et al., Radiation damage to advanced photon source undulators, in: Proceedings of 2005 PAC, Knoxville, TN, p. 4126.
[2] T. Bizen, et al., Nucl. Instr. and Meth. A 467–468 (2001) 185.
[3] T. Bizen, et al., Nucl. Instr. and Meth. A 515 (2003) 850.
[4] T. Bizen, et al., Radiation damage in magnets for undulators at low temperature, in: Proceedings of EPAC 2004, Lucerne, Switzerland, p. 2092.
[5] J. Spencer, et al., Permanent magnets for radiation damage studies, in: Proceedings of 2003 PAC, Portland, OR, p. 2180.
[6] VECTOR FIELDS software for electromagnetic design.